Boundary-Layer Meteorol (2009) 131:403–423
DOI 10.1007/s10546-009-9378-2

ARTICLE

The Influence of Thermally-Induced Mesoscale Circulations on Turbulence Statistics Over an Idealized Urban Area Under a Zero Background Wind

Weiguo Wang

Received: 29 August 2007 / Accepted: 23 March 2009 / Published online: 5 April 2009

Abstract The influence of mesoscale circulations induced by urban-rural differential surface sensible heat flux and roughness on convective boundary-layer (CBL) flow statistics over an isolated urban area has been examined using large-eddy simulation (LES). Results are analyzed when the circulations influence the entire urban area under a zero background wind. For comparison, the CBL flow over an infinite urban area with identical urban surface characteristics under the same background meteorological conditions is generated as a control case (without circulations). The turbulent flow over the isolated urban area exhibits a mix of streaky structure and cellular pattern, while the cellular pattern dominates in the control case. The mixed-layer height varies significantly over the isolated urban area, and can be lower near the edge of the urban area than over the rural area. The vertical profiles of turbulence statistics over the isolated urban area vary horizontally and are dramatically different from the control case. The turbulent kinetic energy (TKE) sources include wind shear, convergence, and buoyancy productions, compared to only buoyancy production in the control case. The normalized vertical velocity variance is reduced compared to the control case except in the central urban area where it is little affected. The low-level flow convergence is mainly responsible for the enhanced horizontal velocity variance in the central urban area, while wind shear is responsible for the additional local maximum of the horizontal velocity variance near the middle of the CBL outside the central area. Parameterizations in the prognostic equation for TKE used in mesoscale models are evaluated against the LES results over the isolated urban area. We also discuss conditions under which the urban-induced circulations occur and when they may affect the entire urban area. Given that urban-induced circulations can influence the entire urban area within hours for an urban area of a realistic size, it is inappropriate to directly apply empirical relations of turbulence statistics derived under horizontally-homogenous flow conditions to an urban area.

W. Wang (✉)
IMSG at National Centers for Environmental Prediction, National Oceanic and Atmospheric Administration, EMC/NOAA Rm 207, 5200 Auth Rd., Camp Springs, MD 20746, USA
e-mail: wang_wg@yahoo.com

Keywords Isolated urban area · Large-eddy simulation · Mixed layer · Thermally-induced mesoscale circulation · Urban boundary layer

1 Introduction

Flow statistics usually vary in the horizontal over an urban area (Ching 1985), and is true even over a horizontally homogeneous urban surface due to the influence of mesoscale circulations induced by urban-rural differences in surface characteristics. Such variations, however, have been ignored in many applications. For example, the mixed-layer turbulence statistical relations developed under horizontally-homogeneous flow conditions are usually applied in urban environments for routine dispersion calculations and parameterizations (e.g., Morrison and Webster 2005). Numerous observational and numerical studies on thermally-induced mesoscale circulation (TMC) over urban areas have been reported in the literature. In contrast, horizontal variations of urban flow statistics have not been well documented, probably due to the difficulties in turbulence measurements under complex urban environments (Roth 2000; Arnfield 2003; Grimmond 2006). In this regard, large-eddy simulation (LES) may provide guidance, and this technique has been used for urban-related studies previously (e.g., Cai 1999; Kanda et al. 2004; Kanda 2006; Xie and Castro 2006). The influence of TMCs on urban flow statistics, however, was not taken into account in these studies, and this is the focus of the present study.

There have been many LES studies regarding the influence of heterogeneous surface forcing on atmospheric boundary-layer (ABL) flow structure (e.g., Hechtel et al. 1990; Hadfield et al. 1991; Shen and Leclerc 1995; Avissar and Schmidt 1998; Gopalakrishnan et al. 2000; Albertson et al. 2001; Kustas and Albertson 2003; Patton et al. 2005). Results from such studies, however, cannot be applied to urban-flow structure for three reasons. First, the aforementioned studies were designed for the parameterization of the effects of subgrid-scale (SGS) landscape heterogeneity on simulations in mesoscale or global models. For this purpose, analyses have concentrated on flow statistics averaged over the entire LES domain, rather than on the horizontal variations of flow statistics. Second, an urban area is usually isolated but most of the aforementioned studies employed periodic surface inhomogeneities of heating rate or topography, e.g., in a sinusoidal fashion, to represent heterogeneous surface forcing. Resulting flow statistics may be unable to represent the impact of abnormal forcing over an isolated area. Third, a longer integration time is needed to simulate the interaction between convective boundary-layer (CBL) turbulence and TMCs than to simulate pure CBL turbulence under horizontally homogeneous flow conditions. The spatial scale of TMCs is $10–10^2$ km, larger than the CBL large eddy scale ($\sim$1 km), and the temporal scale is hours, longer than a large-eddy turnover time ($\sim$15 min). The integration time needs to be at least several TMC turnover times, ensuring that the CBL flow reaches a quasi-steady state and flow statistics are meaningful. For example, analytical results suggest that the influence of TMCs may extend to the free atmosphere (Dalu and Pielke 1993). Avissar and Schmidt (1998) simulated a CBL with a surface inhomogeneity on the scale of 40 km and found that the domain-averaged potential temperature and heat flux vertical profiles considerably depart from those of a typical homogeneous CBL in the quasi-steady state (after a 4.5-h integration). Later, Letzel and Raasch (2003) pointed out that oscillations of the domain-averaged kinetic energy may occur when TMCs develop on scales larger than 5 km, suggesting that an integration time longer than that used by Avissar and Schmidt (1998) is needed for the flow to reach an equilibrium state with inhomogeneous surface forcing. Their study even questioned whether such a quasi-steady state still holds for large-scale heterogeneity. Given

that urban areas (and TMCs) usually occur on spatial scales of 10 km or larger, it is necessary to examine whether a quasi-steady state can be reached.

We present a case study that employs LES to analyze the influence of TMCs on CBL turbulence statistics over an isolated urban area under zero background wind conditions. To highlight the influence, the urban surface is assumed to be homogeneous. These LES experiments have been carefully designed to ensure that the urban area is isolated and both TMCs and turbulence are mutually interactive (Sect. 2). This is the novel aspect of this investigation, since previous LES studies on the urban ABL failed to simulate the TMCs, let alone their influence on turbulence. The horizontal variations of CBL turbulence statistics are analyzed, with emphasis on differences in turbulence statistics and velocity-variance budgets with and without the presence of TMCs (Sect. 3). In Sect. 4, parameterizations in the prognostic equation for turbulent kinetic energy (TKE) used in mesoscale models are evaluated based on LES results. In addition, a scaling analysis is presented, which estimates the conditions under which TMCs appear and when they affect CBL turbulence statistics over an urban area. Finally, a summary is given in Sect. 5.

2 Materials and Methods

2.1 Numerical Model

The numerical model described in Bryan and Fritsch (2002) is used with modifications that consider the urban-induced forcing in the momentum and heat equations (Wang and Davis 2008; Wang 2009). The model solves the Navier-Stokes equations with the third-order Runge-Kutta time-integration scheme, the fifth-order horizontal advection scheme, and the third-order vertical advection scheme. The staggered Arakawa C grid (Arakawa and Lamb 1977) is used.

The simple bulk urban canopy parameterization proposed by Brown and Williams (1998) is used to represent urban effects, with the urban area consisting of built-up areas (e.g., buildings, roads) and park areas. The built-up area fraction is denoted by $f_{\text{built-up}}$ and the park area fraction by $f_{\text{park}} (= 1 - f_{\text{built-up}})$. The built-up area fraction is further divided into the (building) roof fraction (f_{roof}) and the street canopy (between buildings) fraction (f_{canopy}). The drag imposed by the urban canopy is included as an additional term in the Novier-Stokes momentum equation,

$$F_i = -f_{\text{roof}} C_d a(z) V u_i, \tag{1}$$

where F_i represents the drag force ($i = 1$, 2, and 3 refer to the longitudinal (x), lateral (y), and vertical (z) directions, respectively. In the following analysis, u, v, and w also refer to wind components in the x, y, and z directions, respectively), C_d is the drag coefficient of the urban canopy, $a(z)$ is the building surface area density profile, V represents the resolved-scale instantaneous scalar wind speed, and u_i is the resolved-scale velocity. The air is warmed or cooled by the building wall and roof, which is considered in the conservation equation of heat by adding a source term,

$$S_\theta = f_{\text{canopy}} \frac{\partial R_c(z)}{\partial z} + f_{\text{roof}} \frac{Q_{\text{roof}}(h)}{\delta z}, \tag{2}$$

where $R_c(z)$ is the net downward radiative heat flux at a level within the street canopy, Q_{roof} is the heat flux at the roof top, h is the height of the roof top, and δz is the vertical grid size at h. R_c is approximated as,

Table 1 Prescribed parameters describing the urban area

Surface type		Fraction	Surface sensible heat flux ($\mathrm{K\,m\,s^{-1}}$)
Built-up area	Building roof area	$f_{\mathrm{roof}} = 0.2$	0.2
	Between-buildings (street canopy)	$f_{\mathrm{canopy}} = 0.5$	0.2
Non-built-up area (e.g. park area)		$f_p = 0.3$	0.055

$$R_c(z) = R_0 \exp\left(-k_e \int_z^h a(z')dz'\right), \tag{3}$$

where R_0 is the net radiative flux at h, and k_e is an extinction coefficient. For simplicity, $a(z)$ is assumed to be homogeneous in the horizontal and varies linearly from 1 on the surface to zero at the urban canopy top level in the vertical; C_d is taken as 0.15 and k_e as 0.1. An evaluation of the above simple urban parameterization can be found in Chin et al. (2005). The SGS turbulence is parameterized after Deardorff (1980) with a modification that considers the effects of the urban canopy on the SGS TKE by adding a source term $S_{TKE} = f_{\mathrm{roof}} C_d a(z) V^3$ to the SGS TKE equation (Patton 1997).

It should be noted that the above parameterization represents bulk urban-rural differences in surface heat flux and roughness in terms of given parameters characterizing an urban area (Table 1). It is not expected to resolve the microscale turbulence structure within the urban canopy, and as a result, the following analyses focus on the CBL flow above the surface layer where the turbulence is relatively well resolved.

2.2 Experimental Set-Up

Experiments are designed for the daytime CBL. Assumptions in the simulations are as follows: first, the atmosphere is dry; second, there is no synoptic wind throughout the whole domain (i.e., zero background wind); third, the ground is flat and is divided into urban and rural areas (Fig. 1), each area being homogeneous. The isolated urban area is one-dimensional (i.e., the urban surface is infinite in the y direction) (Fig. 1).

The simulation domain of the primary experiment (E4, see Table 2) is 150 km × 6 km with 3000 × 120 nodes in the x and y directions, respectively, and a horizontal grid size of 50 m. The urban size, characterized by the length (D) of the urban area in the x direction, is 15 km. In the vertical direction, 84 nodes are used, with the top of the domain at 2,408 m; the vertical grid size is 2 m below 60 m and 58 m above 900 m, and varies linearly with height between 60 and 900 m. To meet the numerical scheme stability criterion for this grid configuration, the timestep is set to 0.5 s. A rigid lid is used as the top boundary condition, with the Rayleigh friction scheme (Durran and Klemp 1983) being used above 1,800 m to absorb spurious gravity waves and reduce the reflection from the upper part of the domain. The Monin-Obukhov similarity is assumed between the surface and the first grid level, with the aerodynamic (ground) roughness length set to 0.05 m. Lateral boundary conditions are cyclic but the simulation domain is sufficiently large in the x direction so that the turbulent flow statistics over much of the rural area are not affected by the presence of the urban area. This ensures that the urban area remains "isolated" under the cyclic boundary conditions. It should be noted that artificial lateral boundary conditions may be

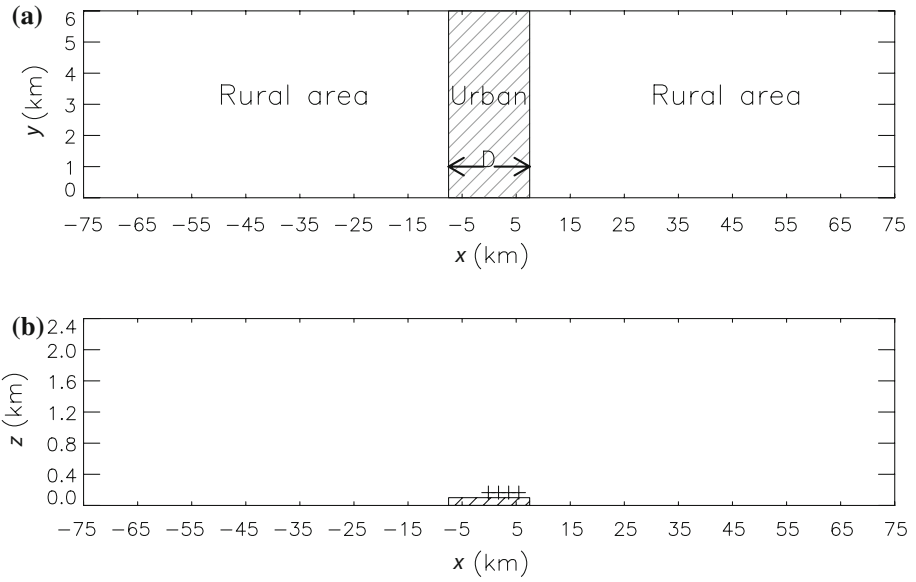

Fig. 1 **a** Schematic of the simulation domain in the horizontal (150 km × 6 km) (not to scale). The hatched area represents a one-dimensional isolated urban area. Both urban surface and rural surface are assumed to be homogeneous, **b** Vertical cross-section of the simulation domain. Four plus signs represent the central locations of the subareas where turbulence statistics are evaluated and their vertical profiles are compared

Table 2 Summary of experiments

Experiment ID	Domain (km^2)	Urban size (km)	Integration time (h)	z_b (m)	z_i (m)	w_* ($m\,s^{-1}$)
E1	6 × 6	∞[a]	10	1,572	1,460	1.97
E2	6 × 6	0[b]	10	1,012	928	1.19
E3	30 × 6	15	10	1,450	1,200	1.84
E4	150 × 6	15	10	1,258	1,005	1.74

[a] Infinite homogeneous urban area
[b] infinite homogeneous rural area
z_b, z_i, and w_* are the ABL height, mixed-layer depth, and convective velocity scale, respectively, averaged over the urban area except for E2 where average is made over the entire rural area

used to replace the cyclic boundary conditions without using a large domain and provide fully developed turbulent inflow and outflow boundary conditions (e.g., Mayor et al. 2002). This method, however, may induce uncertainty and, therefore, has not been adopted in our study.

The atmosphere is initialized uniformly in the horizontal with a weakly stable potential temperature gradient of 0.5 $K\,km^{-1}$ from the ground up to 500 m and a strong capping inversion above (with a potential temperature gradient of 9.8 $K\,km^{-1}$). To trigger the turbulence in the model, random potential temperature perturbations (<0.1 K) are imposed to the lowest two levels. A constant heating rate at the bottom of the domain for each area is prescribed, and the surface sensible heat fluxes over the built-up area (e.g., roof and road, $F_{\text{built-up}}$) and over the rural area (F_{rural}) are prescribed as 0.2 and 0.055 $K\,m\,s^{-1}$, respectively (Table 1).

The surface sensible heat flux over the park area is assumed to be equal to that over the rural area, and the net radiative heat flux (R_0) at the top of the street canopy is assumed to be $0.05\,\mathrm{K\,m\,s^{-1}}$. The fraction of the built-up area is 0.7, of which the building roof fraction is 0.2. Therefore, the imposed heat flux from the ground and roof surface in the lower boundary over the urban area is $0.1565\,\mathrm{K\,m\,s^{-1}}(= (f_{\mathrm{canopy}} + f_{\mathrm{roof}})F_{\text{built-up}} + (1 - f_{\text{built-up}})F_{\mathrm{rural}})$. The total heating from the building wall, $f_{\mathrm{canopy}}(R_c(h) - R_c(0))$, is about $0.0093\,\mathrm{K\,m\,s^{-1}}$ for $h = 20\,\mathrm{m}$. The Coriolis parameter is set to $10^{-4}\mathrm{s}^{-1}$.

Results from three other experiments (Table 2) are also analyzed for comparison. E1 and E2 are seen as two control simulations, where E1 simulates the CBL flow over an infinite homogeneous urban area as described in Table 1, and E2 simulates the CBL flow over an infinite homogeneous rural area. E3 examines the effects of the domain size on the simulations in comparison with E4. The surface characteristics over the urban and rural areas in E3 (and E4) are identical to those in the control urban case (E1) and the control rural case (E2), respectively. TMCs are formed in all experiments except for E1 and E2. Each simulation runs for 10 h, approximately 10 TMC turnover times and about 60 mean large-eddy turnover times (z_b/w_*, where z_b is the ABL height over the urban area and w_* is the convective velocity scale), ensuring statistics are meaningful.

2.3 Averaging

A variable f is partitioned into two components after its temporal trend is linearly removed,

$$f(x, y, z, t) = \langle f \rangle(z) + f_d(x, y, z, t), \tag{4}$$

where the notation $\langle\ \ \rangle$ represents an average over (x, y, t) at height z over the entire urban area, and f_d is the deviation from that average. To identify TMCs, f_d is further partitioned into two components,

$$f_d(x, y, z, t) = [f_d]_y(x, z) + f''(x, y, z, t), \tag{5}$$

where the notation $[\ \ ]_y$ (or only subscript y) represents an average over (y, t) at (x, z), and f'' is the background turbulence component.

2.4 Temporal Oscillations

Letzel and Raasch (2003) found that temporal oscillations in the boundary layer occur if TMCs on the scales of 5 km or more develop. This phenomenon should be taken into account when the length of the model integration time is determined for obtaining meaningful turbulence statistics of the ABL over a heterogeneous surface. In other words, the length of the integration time should be selected to ensure that the turbulent ABL can be maintained in a quasi-steady state at least for several large-eddy or TMC turnover times without the impacts of possible temporal oscillations. To examine if temporal oscillations occur during the 10-h integrations in our experiments, Fig. 2 shows the time series of the flow kinetic energy (KE) $\left(= \frac{1}{2}\sum_{i=1}^{3} u_{id}^2\right)$ averaged over the entire column above the urban area for each experiment. In the two control cases (E1 and E2), the averaged KE increases nearly linearly with time after the first hour until the end of the integration due to the growth of the boundary layer in the absence of subsidence. The temporal oscillation of the averaged KE appears after the fourth hour of the integration in E3. Such an oscillation, however, does not occur in E4. It is found that the ABL turbulence statistics over 15% of the rural area (i.e., about 25 km

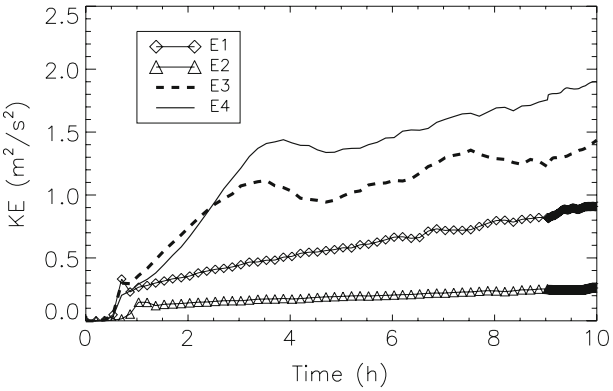

Fig. 2 Time series of kinetic energy (KE) averaged over the column above the urban area for each experiment (Table 2)

in the x-direction) in E4 are identical to those in the control rural case (E2) during the 10-h integration (figures not shown). In other words, the ABL over a part of the rural area in E4 is unaffected by the presence of the urban area.[1] In contrast, the statistics over all the rural area in E3 are affected by the urban area, and the only difference between the two experiments is that E4 has a larger domain than E3. An explanation for the occurrence of the oscillation found in E3 lies in the interaction of meteorological fields on the two sides of the urban area through the cyclic lateral boundary conditions. The disturbed wind, horizontal gradients of temperature and pressure developed on the two sides of the urban area appear in opposite directions and they mutually interact through the cyclic lateral boundary conditions after a period of time since the integration starts. This is similar to the discussion in Letzel and Raasch (2003), which explains the ABL kinetic energy temporal oscillation over a sinusoidal variation of surface heat flux in space. The comparison between E3 and E4 suggests that the temporal oscillation may not occur in our experiments so long as the domain is large enough, so that the disturbed meteorological fields cannot interact through the cyclic lateral conditions.

In addition, Fig. 2 shows that the averaged KE in E4 increases nearly linearly with time after the fifth hour (i.e., approximately 30 large-eddy turnover times and five TMC turnover times) until the end of the integration. The averaged KE normalized by the time-varying w_*^2 is nearly constant, suggesting that the flow has reached the quasi-steady state. Results between hours 9 and 10 are analyzed and reported in the next section, where TMCs are fully developed over the entire urban area, with the inward fronts from both sides of the urban area reaching the urban centre.

3 Results and Comparisons

Results shown in this section are primarily from E4 (the isolated urban case) and E1 (the control infinite homogeneous urban case) in order to highlight the influence of TMCs.

[1] This indicates that the urban area can be considered to be "isolated".

3.1 Urban TMCs

To illustrate TMCs, Fig. 3 shows the horizontal velocity, $[u]_y$, and vertical velocity, $[w]_y$, in E4 averaged over the last 1 h of the integration. The TMCs, appearing mostly within the ABL, are seen as two counter-rotating cells that coincide over the central urban area. In the lower part of the ABL, cold air travels from the rural area towards the urban area at an increasing speed. The inward wind speed is reduced when air travels over the urban surface both due to the decreased horizontal pressure gradient and due to the urban canopy drag. The air approaching from the two sides rises over the central urban area and is deflected outward in the upper part of the ABL. The maximum inward and outward wind speeds appear near the edge of the urban area (about 1.5 km$(0.1D)$ from the edge). Strong convergence and divergence appear within the area 2 km from the urban centre, with the maximum mean vertical velocity being nearly 1 m s^{-1}; this significantly affects local turbulence statistics (see Sect. 3.5).

3.2 Urban Thermal Structure

The TMCs significantly affect the boundary-layer thermal structure over the isolated urban area. The low-level inward flow advects colder air from the rural area into the urban area, while the high-level outward flow advects warmer air away from the urban centre to the rest of the urban area. As a result, air temperature increases in the upper part of the ABL outside the central urban area compared with E1, while it decreases in the lower part of the ABL. This results in a less unstable layer or a weakly stable layer in the upper ABL (Fig. 3c) and can weaken or suppress the convective mixing. In addition, the thermal structure varies in the horizontal. This can be illustrated by the horizontal variations of the local ABL top height (z_{by}) and mixed-layer height (z_{iy}); $z_{by}(x)$ is defined as the level where the maximum vertical potential temperature gradient occurs over the $y-z$ cross-section at a given distance (x) from the urban centre, while $z_{iy}(x)$ is defined as the level of the most negative buoyancy flux. The magnitude of $z_{by}(x)$ is smaller than that in the case with the infinite urban area (E1) and larger than that in the case with the infinite rural area (E2). The rural-urban difference of z_{by} in E4 is mainly due to the larger heating rate over the urban surface than over the rural surface and has been observed in field experiments (Spangler and Dirks 1974; Wong and Dirks 1978; Ching 1985; Briggs 1988; Angevine et al. 2003; Banta and White 2003). The spatial variation of z_{by} over the urban area is negligible. This, however, is not the case for z_{iy}; the highest z_{iy} value appears in the central urban area, while z_{iy} near the edge of the urban area can be as low as 2/3 of that over the central urban area, and can be lower than that over the rural area. The values of z_{iy} and z_{by} are nearly equal in the central urban area, similar to the two control cases (E1 and E2, without the presence of TMCs). Their differences increase with the distance from the centre due to the horizontal advection as described in Sect. 3.1.

3.3 Instantaneous Flow Structure

Compared with the two control cases (E1 and E2), the TMCs modify the turbulent structure of the ABL over the isolated urban area because wind shear and convergence are additional TKE sources. An instantaneous horizontal slice of the vertical velocity distribution at 100 m above the ground in E4 is shown in Fig. 4a, exhibiting a flow pattern with a mix of streaky structure and cellular patterns. The elongated streaky structure of the flow is noticeable over

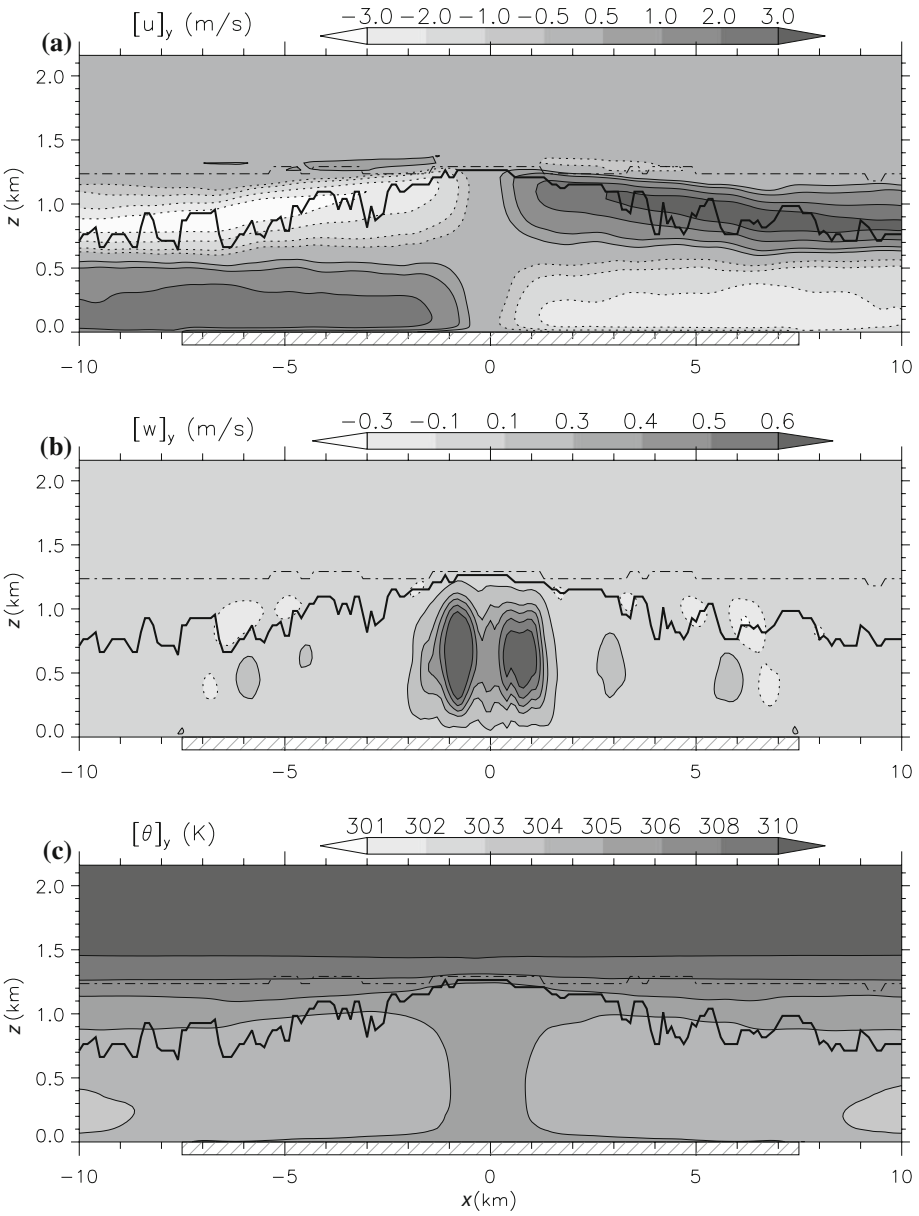

Fig. 3 (**a**) y-averaged and temporally-averaged horizontal velocity $[u]_y$ as a function of distance from the urban centre and height, (**b**) vertical velocity $[w]_y$, and (**c**) potential temperature $[\boldsymbol{\theta}]_y$. The dash-dot line denotes the ABL top. The thick solid line denotes the mixed-layer top. Dotted contours denote negative velocity values and solid contours denote positive velocity values

the entire urban area due to the combined effects of buoyancy and wind shear on turbulence (Moeng and Sullivan 1994). In contrast, the turbulence is generated mainly by buoyancy in the two control cases (without the TMC presence), and, hence, the primary feature of the flow structure is the organized cellular pattern over the entire horizontal domain (Fig. 4b, c).

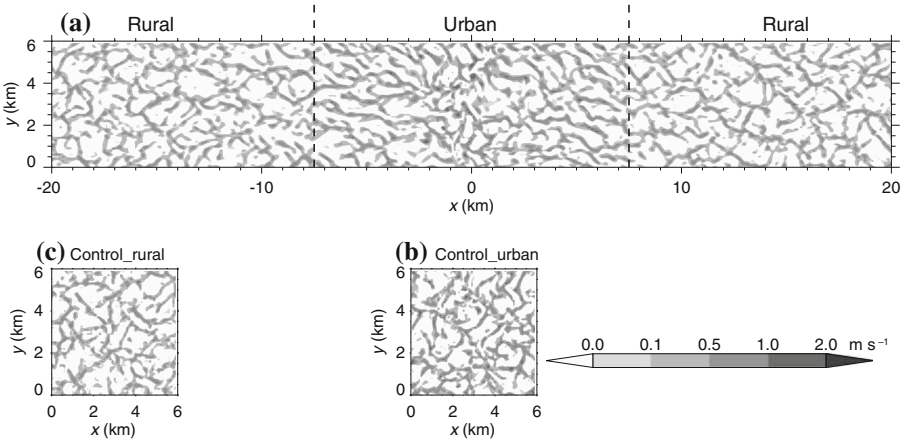

Fig. 4 (**a**) Instantaneous horizontal slices of vertical velocity at $z = 100$ m over part of the simulation domain at the last timestep of the LES run for the isolated urban case (E4), (**b**) the control rural case (E2), and (**c**) the control urban case (E1). Only positive values are shown

3.4 Horizontally-Varied Turbulence Statistics Over the Isolated Urban Area

In order to examine the spatially-varied background turbulence over the isolated urban area, statistics are calculated over the y direction and the last 1 h of the integration in four sub-areas, namely, $x = [-0.5, 0.5]$, $[1, 2]$, $[4, 5]$, and $[6, 7]$ km (Fig. 1b). The ABL structure over the first sub-area is characterized by strong convergence and divergence, while the ABL structure over the other three sub-areas is characterized by strong horizontal wind shear. In the following analyses, we use $x = 0$, 1.5, 4.5, and 6.5 km, to label the vertical profiles averaged over the four sub-areas, respectively.

The shape of the vertical profile of potential temperature over the central urban area ($x = 0$) in the isolated urban case (E4) is nearly identical to that in the control urban case (E1) except that the mixed-layer height is 15% lower (Fig. 5a). Farther from the urban centre, the vertical gradient of potential temperature increases in the upper part of the urban ABL. Figure 5b shows that the inward flow and outward (returning) flow each occupy nearly half of the ABL depth in E4. The large vertical gradients of the horizontal wind appear in the middle part of the ABL in addition to near the surface and the ABL top. The mean vertical velocity appears to be positive within the ABL near the central urban area (Fig. 5c), and increasing with height in the lower part of the ABL (i.e., the horizontal flow is convergent) and decreasing in the upper part (i.e., the horizontal flow is divergent). The magnitude of w decreases with the distance from the urban centre. This is also true for the depth of the layer having positive w values.

Figure 5d, e show the vertical profiles of the velocity variances normalized by the square of the local convective velocity scales (i.e., $w_{*y} = \left(g F_0 z_{by}/\theta_0\right)^{1/3}$, where F_0 is the surface heat flux, g is the gravitational acceleration, and θ_0 is the air potential temperature near the surface). In E1, the horizontal velocity variance is nearly invariant from 0.2 to 0.8 z_b, with the local maximum values appearing near the surface and the ABL top (grey lines in the figure). In E4, the peak value of the horizontal velocity variance near the surface (around 0.1 z_b) at $x = 0$ is larger than that in E1 by a factor of 2. The horizontal velocity variance decreases with height from 0.1 to 0.7 z_b, and increases with height above 0.7 z_b, with another local

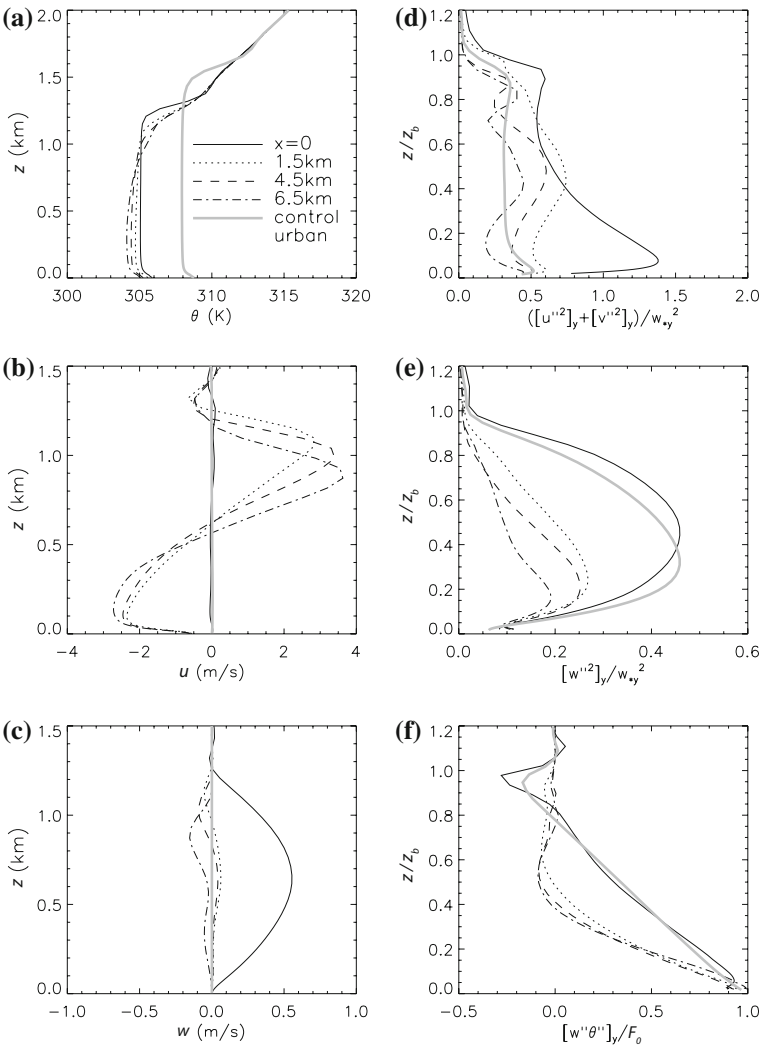

Fig. 5 (**a**) Vertical profiles of the potential temperature averaged over the y direction and the last 1 h of the integration at $x = 0$, 1.5, 4.5, and 6.5 km from the urban centre over the urban area in the isolated urban case (E4); results from the control urban case E1 (grey line) are also shown for comparison, (**b**) mean horizontal velocity, (**c**) mean vertical velocity, (**d**) normalized horizontal-velocity variance, (**e**) normalized vertical velocity variance, and (**f**) normalized buoyancy flux

maximum appearing at $0.9\,z_b$. The significantly enhanced horizontal velocity variance in the lower part of the ABL is mainly attributed to the strong convergence of the horizontal flow in the central urban area (see Sect. 3.5). This is because vortex stretching (convergence) acts to enhance the vorticity of turbulence (and hence the turbulence intensity). Outside the central urban area, a local maximum of the horizontal velocity variance appears near the middle of the ABL due to the vertical shear of the horizontal wind (Fig. 5b), which does not appear in the control case (E1).

Compared with E1, the normalized vertical turbulent velocity variance is significantly reduced above $0.1z_b$ except for the central urban area (Fig. 5e). The ABL is less convective at $x = 1.5, 4.5$, and 6.5 km than in E1 or in the central urban area ($x = 0$). Therefore, the buoyancy, which is a major source of turbulence in the vertical direction, is reduced compared with that in E1. In the central urban area, the shape of the profile of the vertical velocity variance and its maximum are nearly the same as those in E1 except that the position of the maximum is higher due to upward advection. This is expected because the vertical thermal structure in the urban centre is nearly unaffected by the TMCs compared with E1 in terms of the mean potential temperature and buoyancy flux profiles (Fig. 5a, f), and the horizontal flow convergence and divergence in the area do not have direct impacts on the velocity variance in the vertical (see Sect. 3.5).

The buoyancy flux profile outside the central urban area ($x = 1.5, 4.5$, and 6.5 km) is significantly different from that in E1, consistent with the thermal structure modified by the TMCs as discussed above. The weakly-stable temperature stratification in the upper part of the ABL (Fig. 5a) suppresses or weakens the growth of turbulence, leading to the smaller (normalized) buoyancy flux. In the central urban area ($x = 0$), the buoyancy flux profile is similar to that in E1 but the ratio of the entrainment to surface buoyancy fluxes, which is about 0.3, is larger than that (0.2) in the control urban case probably due to strong mean upward motion that enhances eddies penetrating into the inversion layer aloft.

The urban TMCs also modify the asymmetry in the distribution of w fluctuations within the ABL. Figure 6 shows the vertical profiles of the skewness of the w fluctuations (S_w) over the infinite homogeneous urban area in E1 and over the isolated urban area in E4. Here, S_w is calculated using the resolvable-scale vertical velocity because SGS contributions to S_w are not available. The negative values of S_w appearing near the surface and in the stable layer aloft may be spurious due to the insufficient model resolution that cannot resolve small eddies (Moeng 1984; Schmidt and Schumann 1989). Turbulence in E1 is driven dominantly by buoyancy and, therefore, the vertical velocity distribution is positively skewed (grey line in Fig. 6), which has been discussed extensively in the literature (Moeng and Rotunno 1990; Moyer and Young 1991). The TMCs modify the magnitude and distribution of S_w mainly through modifying the eddy structure (Fig. 4), the local temperature stratification, and turbulence intensity (Fig. 5) over the isolated urban area. In the central urban area ($x = 0$), S_w within the ABL appears to be less positive than that in E1. An explanation is that stronger turbulence in the horizontal direction (Fig. 5) makes updrafts more diffusive horizontally and, therefore, the updrafts occupy larger areas (i.e., less skewed) at a given height. Over all the four sub-areas, S_w increases with height in the lower part of the unstable layer and reaches the maximum value near the top of the unstable layer. This behavior is similar to that in the control case (Moeng and Rotunno 1990; Moyer and Young 1991). In the upper part of the ABL over the sub-areas of $x = 1.5, 4.5$, and 6.5 km, S_w is much smaller than that in E1 because the organized updrafts are weakened or lose their kinetic energy when they move into the less unstable or slightly stable layer (Fig. 5a).

3.5 Velocity Variance Budget Analysis

To understand the mechanisms of the influence of the TMCs on turbulence statistics, individual terms in the budget equations for the variances of wind velocity components are analyzed based on LES results, giving insights of benefit to model parameterizations.

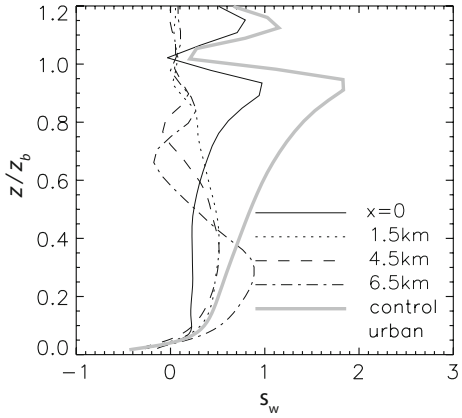

Fig. 6 Vertical profiles of the skewness of the vertical velocity at different locations ($x = 0$, 1.5, 4.5, and 6.5 km) from the isolated urban case. The grey line is for the control (infinite) urban case (E1)

The budget equation for the vertical velocity variance reads,

$$\frac{1}{2}\frac{\partial \overline{w'^2}}{\partial t} = -\frac{1}{2}\overline{U}_j\frac{\partial \overline{w'^2}}{\partial x_j} + \frac{g}{\theta}\overline{w'\theta'} - \overline{w'^2}\frac{\partial \overline{W}}{\partial z} \underbrace{-\overline{u'w'}\frac{\partial \overline{W}}{\partial x} - \overline{v'w'}\frac{\partial \overline{W}}{\partial y}}_{\text{IV}} + \underbrace{\overline{\frac{p'}{\bar{\rho}}\frac{\partial w'}{\partial z}} - \frac{1}{\bar{\rho}}\frac{\partial \overline{w'p'}}{\partial z} - \frac{\partial \overline{u'_j w'^2}}{\partial x_j}}_{\text{V}} - \varepsilon_w \tag{6}$$

I II III IV V VI

where the overbar denotes the ensemble average and the prime denotes the deviation from the average. $\overline{U}_j$ ($j = 1, 2, 3$) or $\overline{U}$, $\overline{V}$, $\overline{W}$ are the mean wind velocity components in the x, y, and z directions, respectively; the repeated index j implies a sum. Also, $\bar{\rho}$ is the mean air density, p' is the pressure perturbation, and ε_w is the viscous dissipation rate of the vertical velocity variance. The six terms on the right-hand side (RHS) of the equation represent the gains or losses of the variance due to the processes of advection by the mean wind (I), buoyancy (II), mean flow convergence (or divergence) (III), mean wind shear (IV), and the redistribution by turbulent transport and pressure perturbation (V), the viscous dissipation (VI), respectively.

Similarly, the budget equation for the horizontal velocity variance reads,

$$\frac{1}{2}\frac{\partial \overline{u_h^2}}{\partial t} = -\frac{1}{2}\overline{U}_j\frac{\partial \overline{u_h^2}}{\partial x_j} \underbrace{-\overline{u'^2}\frac{\partial \overline{U}}{\partial x} - \overline{v'^2}\frac{\partial \overline{V}}{\partial y}}_{\text{III}} \underbrace{-\overline{u'v'}\frac{\partial \overline{U}}{\partial y} - \overline{u'w'}\frac{\partial \overline{U}}{\partial z} - \overline{u'v'}\frac{\partial \overline{V}}{\partial x} - \overline{v'w'}\frac{\partial \overline{V}}{\partial z}}_{\text{IV}}$$

$$\underbrace{+\overline{\frac{p'}{\bar{\rho}}\frac{\partial u'}{\partial x}} - \frac{1}{\bar{\rho}}\frac{\partial \overline{u'p'}}{\partial x} + \overline{\frac{p'}{\bar{\rho}}\frac{\partial v'}{\partial y}} - \frac{1}{\bar{\rho}}\frac{\partial \overline{v'p'}}{\partial y} - \frac{\partial \overline{u'_j u_h^2}}{\partial x_j}}_{\text{V}} - \varepsilon_h, \tag{7}$$

VI

where $\overline{u_h^2}$ is the sum of the variances for wind components in the x and y directions, i.e., $\overline{u'^2 + v'^2}$, and ε_h is the viscous dissipation rate of $\overline{u_h^2}$. The numbered terms on the RHS of Eq. 7 have the same physical meanings as those in Eq. 6 except for $\overline{u_h^2}$. The buoyancy term (term II), which acts only in the vertical direction, does not appear in this equation.

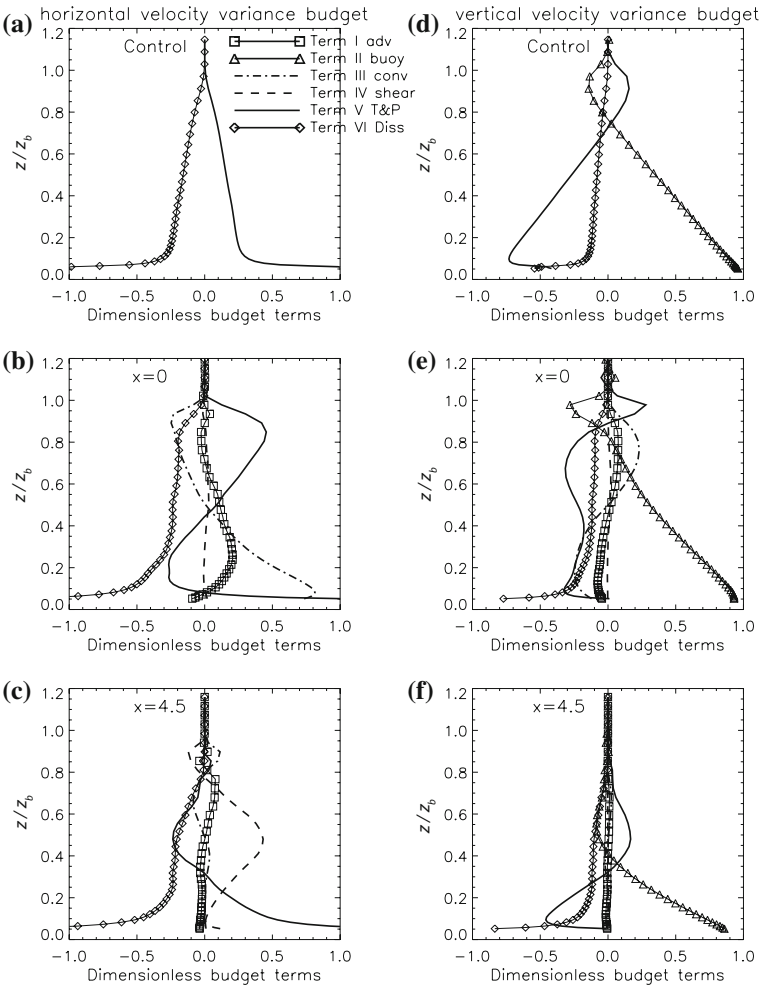

Fig. 7 (**a**) Vertical profiles of the horizontal velocity variance budget terms normalized by w_*^3/z_b for the control urban case (E1), (**b**) at the urban centre $x = 0$ in the isolated urban case (E4), (**c**) at $x = 4.5$ km from the urban centre in the isolated urban case (E4), (**d**–**f**) are same as (**a**–**c**) respectively, except for the vertical velocity budget terms

Figure 7 shows the vertical profiles of the budget terms over the infinite and homogeneous urban area (E1) and over two sub-areas in the isolated urban area respectively representing the convergence/divergence and shear flow regimes (E4). As no mean flow is present in E1, the redistribution term (V) and dissipation term (VI) are balanced in the $\overline{u_h^2}$ budget equation (Fig. 7a), while the buoyancy term (II), redistribution term (V), and dissipation term (VI) are balanced in the $\overline{w'^2}$ budget equation (Fig. 7d). The sole TKE source is the buoyancy production of $\overline{w'^2}$ in E1. Some of that production is dissipated in Eq. 6 and the remainder is transferred to the horizontal component of TKE and/or is redistributed spatially through the turbulence and pressure transport term. The $\overline{w'^2}$ loss is mainly due to the negative buoyancy in the entrainment zone, which is balanced by the redistribution term.

With the influence of TMCs, TKE is gained by the productions of mean wind shear and convergence in addition to buoyancy. In the central urban area ($x = 0$) with strong flow convergence and divergence, all terms in Eqs. 6 and 7 except the mean wind shear production term are of the same magnitude and are important in maintaining the budgets. In the lower part of the ABL, the gain of $\overline{w'^2}$ is due to buoyancy, while the loss of $\overline{w'^2}$ is due to dissipation, advection (mostly in the vertical), and the divergence of the mean vertical velocity. In the upper part of the ABL, the gain of $\overline{w'^2}$ is due to vertical advection of $\overline{w'^2}$ and the mean vertical-velocity convergence, in addition to buoyancy. With regard to the $\overline{u_h'^2}$ budget, the gain of $\overline{u_h'^2}$ is mainly due to the horizontal flow convergence and advection in the lower part of the ABL, except near the surface where the redistribution term is a significant source term, while the loss of $\overline{u_h'^2}$ is due to dissipation and redistribution. In the upper part of the ABL, the horizontal flow divergence contributes to the loss of $\overline{u_h'^2}$, in addition to the dissipation. The shear production term is negligible because the vertical gradient of the horizontal wind is small in the central urban area (Fig. 5). In the area $x = 4.5$ km, the $\overline{w'^2}$ budget is not much affected in terms of the relative importance of the budget terms, compared with that in E1. This, however, is not the case for the $\overline{u_h'^2}$ budget. The mean wind shear term contributes to the gain of $\overline{u_h'^2}$ in the middle part of the ABL, which does not appear in E1. In the lower part of the ABL, the wind shear and redistribution terms are source terms, which are mainly balanced by the dissipation term. In the upper part of the ABL, the gain of $\overline{u_h'^2}$ is due to mean wind shear and advection, while the loss is due to divergence, in addition to redistribution and dissipation.

4 Discussion

4.1 Evaluation of Parameterizations in the TKE Equation for Mesoscale Models

TKE is a prognostic variable in mesoscale models, with several terms in the TKE prognostic equation being parameterized. It is instructive to examine how well those parameterizations represent the urban flow. The shear production (SP) term, turbulence and pressure transport (TP) term, and dissipation rate (DR) term are usually parameterized as,

$$SP = -\overline{u'w'}\frac{\partial \bar{U}}{\partial z} - \overline{v'w'}\frac{\partial \bar{V}}{\partial z} = l_M\sqrt{2E}\left[\left(\frac{\partial \bar{U}}{\partial z}\right)^2 + \left(\frac{\partial \bar{V}}{\partial z}\right)^2\right], \tag{8}$$

$$TP = -\overline{w'E'} - \frac{1}{\bar{\rho}}\frac{\partial \overline{w'p'}}{\partial z} = l_E\sqrt{2E}\frac{\partial E}{\partial z}, \tag{9}$$

$$DR = \varepsilon = \frac{E^{3/2}}{l_e}, \tag{10}$$

where E is TKE($= 0.5(\overline{u'^2} + \overline{v'^2} + \overline{w'^2})$), l_M and l_E are the length scales for the exchanges of momentum and TKE, respectively, and l_e is the dissipation length scale. In many closure models, these length scales are assumed to be proportional to a master length scale (l) (Mellor and Yamada 1982), i.e., $l_M = C_M l$, $l_E = C_E l$, and $l_e = C_e l$, where C_M, C_E, and C_e are empirical constants or functions of stability tuned to available observations. A commonly-used and simple algebraic expression for l is,

$$l = l_0 \frac{\kappa z}{\kappa z + l_0}, \tag{11}$$

where $l_0 = 0.1 \int_0^\infty \sqrt{E} z dz / \int_0^\infty \sqrt{E} dz$, and κ is the Karman constant (0.4). This formulation was proposed by Blackadar (1962) for the momentum mixing length in a neutral atmosphere, but it has been often used in mesoscale and large-scale atmosphere models for wind, temperature, and specific humidity under various atmospheric conditions.

We calculated SP, TP, and DR over each sub-area of the isolated urban area based on the parameterizations (i.e., the far RHS of Eqs. 8–10) by assuming that l_M, l_E, and l_e were equal to l. Results are denoted by SP1, TP1, and DR1, respectively. Meanwhile, SP, TP, and DR are also calculated directly from the LES-resolved and SGS variables. Comparisons of the results from the two calculations are shown in Fig. 8. C_M, C_E, and $1/C_e$ are equal to the ratios of LES-derived SP, TP, and DR to SP1, TP1, and DR1, respectively, so that the parameterizations can reproduce the LES-derived results. Figure 8a suggests that C_M varies between 0 and 2. This is comparable to the derivation by Mellor and Yamada (1982) showing that C_M varies from zero under stable conditions to two under very unstable conditions. For the TP term, C_E values are largely scattered (Fig. 8b). Despite this, there is a tendency that the parameterized TP can reasonably simulate LES results by taking C_E to be 0.25 (i.e., mean value) for the wind-shear-flow regime ($x = 1.5$, 4.5, and 6.5 km). As a comparison, Mellor and Yamada (1982) suggested that C_E is taken as 0.2 for the neutral flow and found that it is not significantly sensitive to stability. In the urban centre ($x = 0$), most C_E values vary from 0 to 2 under the free convection condition and there is no tendency that a universal value exists for C_E. This may be explained as follows: first, the local flux-gradient relation does not work well under the free convection condition. Second, the master length scale (Eq. 11) was developed for a neutral atmosphere where turbulence is generated predominantly by mechanical production (wind shear). In contrast, turbulence is generated predominantly by buoyancy under the free-convection condition where the mixing length is of the order of the CBL depth. C_e is approximately 16 at the urban centre, and decreases to approximately 8, 5, and 3 at $x = 1.5$, 4.5, and 6.5 km, respectively, as the ABL becomes less convective. This suggests that the master length scale needs to be further adjusted to represent the dissipation length scale under the more unstable flow regime. As a comparison, Mellor and Yamada (1982) suggested that $C_e = 5.86$ for a neutral flow.

In addition, it is noticed that the convergence/divergence terms (i.e., term III in Eqs. 6 and 7) in the budget equations have been ignored in the parameterizations of the TKE equation used in most mesoscale models. This could result in significant errors in predicting TKE in strong convergence or divergence areas, given the importance of the terms as shown in Sect. 3.5. Therefore, representing the effects of convergence/divergence in the TKE equation is desirable.

4.2 When does the Influence of TMCs Matter?

In Sect. 3, we have compared turbulence statistics over the isolated urban area with those over an infinite homogeneous urban area (i.e., without TMCs). It is natural to ask the following two questions: (1) When can TMCs affect the entire urban area after they start to develop in the morning? (2) Over what area is the influence of TMCs negligible so that the empirical CBL statistical relations developed under horizontally homogeneous conditions can still apply? A simple scaling method is used to answer the questions.

Briggs (1988) derived the characteristic urban-induced horizontal velocity scale, U, under zero or light background wind conditions, i.e.,

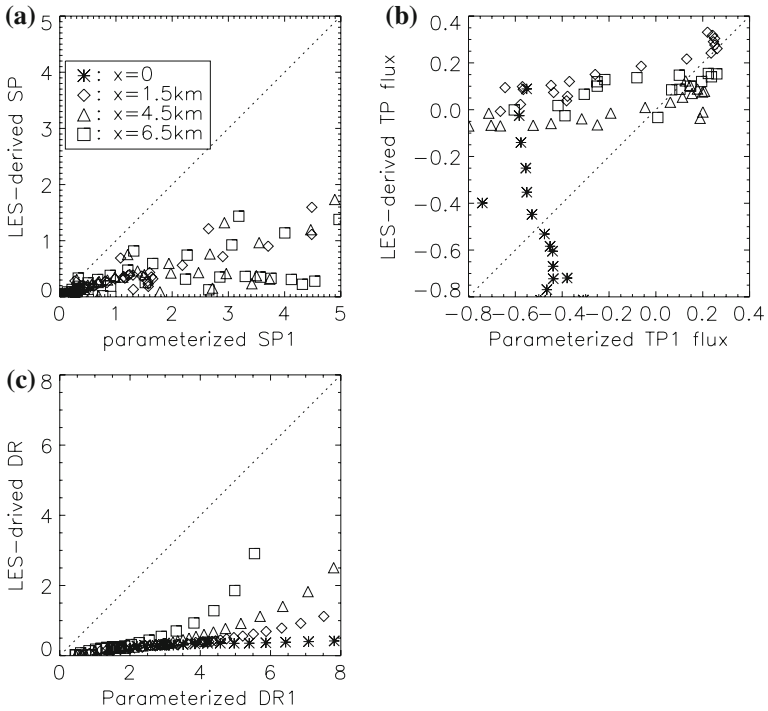

Fig. 8 (**a**) Comparison of LES-derived and parameterized results for the shear production (SP) term. (**b**) TKE and pressure (TP) flux, and (**c**) dissipation rate (DR). The dotted line is the 1:1 line. All coefficients are set to 1 in the parameterizations (Eqs. 8–10) when computing SP1, TP1, and DR1. C_M, C_E, and $1/C_e$ are equal to the ratios of SP/SP1, TP/TP1, and DR/DR1 so that the parameterizations reproduce LES results. See text for details

$$U = \left(\frac{dg\Delta F_0}{4\theta_0} \right)^{1/3}, \tag{12}$$

where ΔF_0 is the difference in surface sensible heat flux over urban and rural areas, and d is the urban size (i.e., D in this study). In deriving U, it has been assumed that all the excess buoyancy flux ΔF_0 is used to increase the buoyancy of an updraft over all the urban area and the resulting horizontal hydrostatic pressure difference creates the inflow wind. The above expression works reasonably well for urban areas[2] with realistic sizes (e.g., $D < 20$ km) under real atmospheric conditions (Wong and Dirks 1978; Briggs 1988). We modified Eq. 12 to consider the temporal dependence of U, before the urban-induced wind front reaches the central urban area, using a time-dependent d, i.e.,

$$d(t) = \min \left(2 \int_{t=0}^{t} U(t)dt, D \right), \tag{13}$$

where t is time, $t = 0$ is the starting time when TMCs develop, $d/2$ is the distance between the edge of the urban area and the inflow wind front position. Here we have assumed that

[2] Here, an urban area is defined by the area in a city where the surface heat flux is significantly larger than the rural area, rather than by administrative divisions.

the excess energy (due to different surface heating rates over urban and rural areas) over a fraction (i.e. d/D) of the urban area is used to fuel the TMCs before the front reaches the central urban area. After the front reaches the centre, the excess energy over all the urban area is used to fuel the TMCs. In this case, U is independent of time and is determined mainly by the size of the urban area and the urban-rural difference in the surface sensible heat flux. The time that it takes for the inflow front to reach the urban centre can be estimated to be D/U_0 with an approximation of $\int_{t=0}^{t} U(t)dt \approx 0.5U(t)t$, where U_0 is the inflow wind speed when $d = D$. Given $D = 15\,\mathrm{km}$, $\Delta F_0 = 0.1\,\mathrm{K\,m\,s^{-1}}$, $\theta_0 = 300\,\mathrm{K}$, it takes approximately 3.6 h for the inflow wind front to reach the urban centre. The influence of the TMCs on local turbulence statistics is negligible over the area within the distance of $(\mathrm{D} - d)/2$ from the urban centre. To test this estimation, we have examined the vertical profiles of the velocity variances and skewness averaged over the four sub-areas between 2.5 and 3 h after the integration starts. It is found that the vertical profiles of velocity variances and skewness in the urban centre ($x = 0$) are nearly identical to those in the control urban case, suggesting that the influence of the TMCs is negligible. By comparison, the statistics over the areas of $x = 1.5$, 4.5, and 6.5 km have been affected, similar to those shown in Sect. 3.

Equation 12 can be used to derive conditions under which TMCs can be formed. From the scaling perspective, the TMCs over an isolated urban area may be noticeably present when the magnitude of the urban-induced organized horizontal velocity is larger than the background turbulent velocity scale (i.e. over the rural area), e.g., $U > w_*$. Thus, we have,

$$\Delta F_0 > \frac{4F_{b0}z_{b0}}{D}, \tag{14}$$

where F_{b0} and z_{b0} are the background surface sensible heat flux and CBL depth, respectively. The critical urban-rural heating difference (i.e., RHS of Eq. 14) increases with the background ABL depth and surface sensible heat flux, and decreases with increasing urban size. Physically, for a smaller urban area, urban-rural differences in horizontal air pressure or temperature can be more easily reduced or eliminated by the mixing of large eddies in the background CBL.

4.3 Limitations

This case study has limitations and can be further improved in the future:

(1) The above analyses are applied only to calm or light background wind conditions. The influence of TMCs on urban flow statistics may vary with the background wind and surface conditions, which has not been examined in this study.
(2) The microscale turbulence within and above the urban canopy is not well resolved in this study due to the bulk urban canopy parameterization and limited grid resolution used near the urban surface. Microscale turbulence over urban-like surfaces has been investigated numerically and experimentally (Cheng and Castro 2002; Kanda et al. 2004; Castro et al. 2006; Kanda 2006), but its impact on ABL flow statistics above the surface layer has not been fully addressed.
(3) The urban surface characteristics have been imposed to be horizontally homogeneous. As a result, the effects of urban surface heterogeneity on flow statistics are not taken into account in the analyses. Such effects could be significant unless the length scale of the heterogeneity is much smaller than the large-eddy scale (Shen and Leclerc 1995; Avissar and Schmidt 1998; Patton et al. 2005).

5 Summary

The turbulent boundary layer over an isolated urban area under a zero background wind has been examined using LES, with the emphasis on the influence of urban-induced TMCs on turbulent flow statistics above the surface layer when the TMCs have been fully developed. To highlight the influence of the TMCs, the urban surface has been assumed to be horizontally homogeneous. The urban ABL with the TMCs is generally less convective than that without the TMCs. The mixed-layer height varies significantly in the horizontal, with the highest value appearing in the central urban area and the lowest value appearing near the edge of the urban area. The flow structure over the isolated urban area exhibits a mix of streaky and cellular patterns. In contrast, only a cellular pattern is found over the infinite and homogeneous urban area (the control urban case without TMCs). The distribution of the vertical velocity fluctuation in the central urban area is generally less positively-skewed than that in the control case.

With the influence of the TMCs, the wind shear and convergence productions are the TKE source terms in addition to the buoyancy production, while the sole TKE source is from the buoyancy production in the control urban case. Turbulence statistics and velocity-variance budgets in two types of flow regimes over the isolated urban area are compared with each other and with those in the control urban case. They are summarized as follows:

(1) In the flow regime with strong wind shear, the horizontal velocity variance varies with height, with a local maximum appearing in the middle part of the ABL in addition to near the surface and ABL top. By comparison, the horizontal velocity variance is nearly invariant in the middle part of the ABL in the control case. The ABL over the isolated urban area is less convective than in the control urban case; this significantly reduces the buoyancy flux and, hence, the vertical velocity variance. The wind-shear production term is mainly responsible for the gain of the horizontal-velocity variance budget in the middle part of the ABL and the negative buoyancy flux is responsible for the loss of the vertical velocity variance in the middle and upper parts of the ABL.
(2) In the flow regime with strong flow convergence and divergence, turbulence is enhanced in the horizontal direction in the lower part of the ABL. In the middle part of the ABL, the horizontal velocity variance decreases with height, compared to being nearly constant in the control case. The shape of the vertical profile of the vertical velocity variance is similar to that in the control case but the peak location is heightened. The vertical advection and convergence/divergence terms play significant roles in maintaining the budget.

Parameterizations in the prognostic equation of TKE for mesoscale models are examined based on the LES results over the isolated urban area. In the flow regime with strong wind shear, the flux-gradient relation may provide reasonable parameterizations by adjusting the mixing length scale. This, however, is not the case for the flow regime with strong convergence and divergence. In addition, the effects of the mean flow convergence and divergence on TKE, which can play a significant role in maintaining the TKE budget, have been ignored in the parameterizations of the TKE equation used in most mesoscale models. This could result in significant errors for simulating the turbulent flow (such as urban flow) with strong convergence and divergence. From the perspective of scaling, conditions under which TMCs appear and when they can influence local turbulence statistics are discussed. Large urban size and a large urban-rural difference in the surface sensible heat flux favour the formation of TMCs. It is inappropriate to directly apply existing ABL statistical relations derived under horizontally homogeneous conditions to isolated urban areas in practice, given that

the TMC front can reach the urban centre within hours. This should be kept in mind for practical dispersion modelling and urban turbulence parameterization. Further investigations under various atmospheric conditions and development of the ABL statistics relations with the influence of TMCs are desirable.

Acknowledgements The author thanks Dr. G. Bryan who provided the model source codes, and thanks reviewers for constructive suggestions. Part of this work was motivated and completed when the author worked in the Pacific Northwest National Laboratory.

References

Albertson JD, Kustas WP, Scanlon TM (2001) Large-eddy simulation over heterogeneous terrain with remotely sensed land surface conditions. Water Resour Res 37:1939–1953. doi:10.1029/2000WR900339

Angevine WM, White AB, Senff CJ, Trainer M, Banta RM, Ayoub MA (2003) Urban-rural contrasts in mixing height and cloudiness over Nashville in 1999. J Geophys Res Atmos 108(D3):4092. doi:4010.1029/2001JD001061

Arakawa A, Lamb V (1977) Computational design of the basic dynamical processes of the UCLA general circulation model. In: Chang J (ed) Methods in computational physics, vol 17. Academic Press, pp 173–265

Arnfield AJ (2003) Two decades of urban climate research: a review of turbulence, exchanges of energy and water, and the urban heat island. Int J Climatol 23(1):1–26. doi:10.1002/joc.859

Avissar R, Schmidt T (1998) An evaluation of the scale at which ground-surface heat flux patchiness affects the convective boundary layer using large-eddy simulations. J Atmos Sci 55(16):2666–2689. doi:10.1175/1520-0469(1998)055<2666:AEOTSA>2.0.CO;2

Banta RM, White AB (2003) Mixing-height differences between land use types: dependence on wind speed. J Geophys Res Atmos 108(D10):4321. doi:4310.1029/2002JD002748

Blackadar AK (1962) The vertical distribution wind and turbulent exchnage in a neutral atmosphere. J Geophys Res 67:3095–3102. doi:10.1029/JZ067i008p03095

Briggs GA (1988) Surface inhomogeneity effects on convective diffusion. Boundary-Layer Meteorol 45(1–2):117–135

Brown MJ, Williams M (1998) An urban canopy parameterization for mesoscale meteorological models. In: Proceedings of second symposium on the urban environment, Albuquerque, NM1998, American Meteorological Society, pp 144–147

Bryan GH, Fritsch JM (2002) A benchmark simulation for moist nonhydrostatic numerical models. Mon Weather Rev 130(12):2917–2928. doi:10.1175/1520-0493(2002)130<2917:ABSFMN>2.0.CO;2

Cai X (1999) Large-eddy simulation of the convective boundary layer over an idealized patchy urban surface. Q J Roy Meteorol Soc 125:1427–1444. doi:10.1256/smsqj.55615

Castro I, Cheng H, Reynolds R (2006) Turbulence over urban-type roughness: deductions from wind-tunnel measurements. Boundary-Layer Meteorol 118(1):109. doi:10.1007/s10546-005-5747-7

Cheng H, Castro IP (2002) Near wall flow over urban-like roughness. Boundary-Layer Meteorol 104(2):229–259. doi:10.1023/A:1016060103448

Chin HS, Leach MJ, Sugiyama GA, Leone JM Jr, Hoyt W, Nasstrom JS, Brown MJ (2005) Evaluation of an urban canopy parameterization in a mesoscale model using VTMX and URBAN 2000 data. Mon Weather Rev 133:2043–2068. doi:10.1175/MWR2962.1

Ching JKS (1985) Urban-scale variations of turbulence parameters and fluxes. Boundary-Layer Meteorol 33(4):335–361. doi:10.1007/BF00116683

Dalu GA, Pielke RA (1993) Vertical fluxes generated by mesoscale atmospheric flow induced by thermal inhomogeneities in the PBL. J Atmos Sci 50:919–926. doi:10.1175/1520-0469(1993)050<0919:VHFGBM>2.0.CO;2

Deardorff JW (1980) Stratocumulus-capped mixed layers derived from a three-dimensional model. Boundary-Layer Meteorol 18(4):495–527. doi:10.1007/BF00119502

Gopalakrishnan SG, Roy SB, Avissar R (2000) An evaluation of the scale at which topographical features affect the convective boundary layer using large eddy simulations. J Atmos Sci 57:336–351

Grimmond CSB (2006) Progress in measuring and observing the urban atmosphere. Theor Appl Climatol 84(1–3):3–22

Hadfield MG, Cotton WR, Pielke RA (1991) Large-eddy simulation of thermally forced circulation in the convective boundary layer. Part I: A small scale circulation with zero wind. Boundary-Layer Meteorol 57:79–114. doi:10.1007/BF00119714

Hechtel LM, Moeng C-H, Stull RB (1990) The effects of nonhomogeneous surface fluxes on the convective boundary layer: a case study using large-eddy simulation. J Atmos Sci 47:1721–1741. doi:10.1175/1520-0469(1990)047<1721:TEONSF>2.0.CO;2

Kanda M (2006) Large-eddy simulations on the effects of surface geometry of building arrays on turbulent organized structures. Boundary-Layer Meteorol 118(1):151–168. doi:10.1007/s10546-005-5294-2

Kanda M, Moriwaki R, Kasamatsu F (2004) Large-eddy simulation of turbulent organized structures within and above explicitly resolved cube arrays. Boundary-Layer Meteorol 112(2):343–368. doi:10.1023/B:BOUN.0000027909.40439.7c

Kustas WP, Albertson JD (2003) Effects of surface temperature contrast on land-atmosphere exchange: a case study from Monson 90. Water Resour Res 39:1159. doi:1110.1029/2001WR001226

Letzel MO, Raasch S (2003) Large eddy simulation of thermally induced oscillations in the convective boundary layer. J Atmos Sci 60(18):2328–2341. doi:10.1175/1520-0469(2003)060<2328:LESOTI>2.0.CO;2

Mayor SD, Spalart PR, Tripoli GJ (2002) Application of a perturbation recycling method in the large-eddy simulation of a mesoscale convective internal boundary layer. J Atmos Sci 59(15):2385–2395. doi:10.1175/1520-0469(2002)059<2385:AOAPRM>2.0.CO;2

Mellor GL, Yamada T (1982) Development of a turbulence closure model for geophysical fluid problems. Rev Geophys Space Phys 20(4):851–875. doi:10.1029/RG020i004p00851

Moeng C-H (1984) A large-eddy-simulation model for the study of planetary boundary-layer turbulence. J Atmos Sci 41:2052–2062. doi:10.1175/1520-0469(1984)041<2052:ALESMF>2.0.CO;2

Moeng C-H, Rotunno R (1990) Vertical-velocity skewness in the buoyancy-driven boundary layer. J Atmos Sci 47(9):1149–1162. doi:10.1175/1520-0469(1990)047<1149:VVSITB>2.0.CO;2

Morrison NL, Webster HN (2005) An assessment of turbulence profiles in rural and urban environments using local measurements and numerical weather prediction results. Boundary-Layer Meteorol 115(2):223–239. doi:10.1007/s10546-004-4422-8

Moyer KA, Young GS (1991) Observations of vertical velocity skewness within the marine stratocumulus-topped boundary layer. J Atmos Sci 48(3):403–410. doi:10.1175/1520-0469(1991)048<0403:OOVVSW>2.0.CO;2

Patton EG (1997) Large-eddy simulation of turbulent flow above and within a plant canopy. PhD dissertation, University of California, Davis

Patton EG, Sullivan PP, Moeng C-H (2005) The influence of idealized heterogeneity on wet and dry planetary boundary layers coupled to the land surface. J Atmos Sci 62(7):2078–2097. doi:10.1175/JAS3465.1

Roth M (2000) Review of atmospheric turbulence over cites. Q J Roy Meteorol Soc 126:941–990. doi:10.1256/smsqj.56408

Schmidt H, Schumann U (1989) Coherent structure of the convective boundary layer derived from large-eddy simulations. J Fluid Mech 200:511–562. doi:10.1017/S0022112089000753

Shen S, Leclerc MY (1995) How large must surface inhomogeneities be before they influence the convective boundary layer structure? A case study. Q J Roy Meteorol Soc 121:1209–1228. doi:10.1002/qj.49712152603

Spangler T, Dirks R (1974) Meso-scale variations of the urban mixing height. Boundary-Layer Meteorol 6(3–4):423–441

Wang W (2009) The influence of topography on single-tower-based carbon flux measurements under unstable conditions: a modeling perspective. Theor Appl Climatol. doi:10.1007/s00704-009-0130-0

Wang W, Davis K (2008) A numerical study of the influence of a clearcut on eddy-covariance flux measurements above a forest. Agric For Meteorol 148:1488-1500. doi:1410.1016/j.agrformet.2008.1405.1009

Wong KK, Dirks RA (1978) Mesoscale perturbations on airflow in the urban mixing layer. J Appl Meteorol 17(5):677–688. doi:10.1175/1520-0450(1978)017<0677:MPOAIT>2.0.CO;2

Xie Z, Castro I (2006) LES and RANS for turbulent flow over arrays of wall-mounted obstacles. Flow Turbul Combus 76(3):291–312. doi:10.1007/s10494-006-9018-6